

# Geometric Realism Without Angular Resolution

## Structural Classification of Multilayer Kubelka–Munk Theory within Radiative Transport

Claude Zeller

*Claude Zeller Consulting LLC, Tillamook, Oregon*  
czeller@ieee.org

### Abstract

Kubelka–Munk (KM) theory provides a two-flux description of radiative transport in layered scattering and absorbing media. Despite its wide use in the coatings, paper, paint, and textile industries, the theory has often been regarded as a phenomenological model whose connection to the full radiative transfer equation (RTE) remains unclear. Under the standard steady-state, plane-parallel, azimuthally symmetric assumptions, we show that multilayer KM theory is exactly a rank-2 Galerkin projection of the RTE onto hemispherical basis functions. The projection is idempotent with an infinite-dimensional kernel, and its rank is preserved under multilayer composition—so no amount of layer stacking can recover angular information discarded by the projection. We derive the KM coefficients as hemispherical moments of the transport operator and compute the projection error for representative scattering media ( $g$  from 0 to 0.85), finding that the reduced optical thickness  $\tau^* = \tau(1 - g)$  governs KM accuracy. The projection-error framework explains the well-documented accuracy of compositional multilayer models in printed media and shows where higher-order methods become necessary. The result places KM theory on rigorous footing as a legitimate—if low-resolution—transport approximation rather than an ad hoc phenomenology.

## 1 Introduction

Two-flux models collapse the full angular distribution of radiance into a pair of scalar fluxes: one going forward, one going backward. It is about the crudest simplification imaginable, and it has been extraordinarily successful. The Kubelka–Munk (KM) model [1, 2], introduced in 1931, is the most widely used instance. It describes a homogeneous scattering-absorbing slab using two parameters—an absorption coefficient  $K$  and a scattering coefficient  $S$ —and yields closed-form expressions for reflectance and transmittance. For decades it has been the workhorse of color science in paints, paper, textiles, and coatings.

The simplicity that makes KM theory useful also makes it suspect. The model cannot distinguish an isotropic scatterer from one with a sharp forward peak. It treats every photon within a hemisphere as interchangeable. Many authors have regarded it as “merely phenomenological” (see, e.g., the discussion in [13]) and have proposed corrections—Saunderson surface corrections [9], path-length multipliers, modified scattering coefficients—that try to put back what the two-flux reduction threw away.

The connection between KM theory and the radiative transfer equation is not itself new. Mudgett and Richards [10] derived KM from the RTE by hemispherical averaging and established that  $K = 2\sigma_a$ . Star et al. [11] and van Gemert and Star [12] refined the treatment for anisotropic

scattering, identifying the backscatter fraction  $\bar{p}_{-+}$  as the bridge between transport and KM scattering coefficients. These derivations are correct and this paper relies on them. What they did not do is identify the hemispherical average as an orthogonal Galerkin projection with a specific rank, kernel, and idempotence structure. That step is what this paper adds, and it yields three results that do not follow from the earlier work: (i) the infinite-dimensional kernel  $\ker(\mathcal{P})$ , which characterizes exactly what KM theory cannot represent; (ii) a rank-preservation theorem explaining why multilayer composition cannot recover the discarded information; and (iii) a projection-error criterion  $\varepsilon$  that quantitatively bounds KM accuracy as a function of the scattering parameters.

A substantial body of work by Hébert, Hersch, and collaborators [4, 5, 6, 7, 8] has developed a powerful compositional framework for predicting the reflectance and transmittance of multilayer specimens using transfer matrices. Each optical element—a scattering layer, an ink film, a refractive interface—is characterized by its reflectances and transmittances. Stacking two elements produces a composite element whose properties follow from summing the infinite geometric series of internal bounces in closed form. They showed that Kubelka’s layering model, the Saunderson correction, and the Williams–Clapper model are all special cases of a single compositional formalism, and that the two-flux matrix approach extends naturally to four-flux and multiflux models when one needs to distinguish collimated from diffuse light. The framework has been validated to high accuracy in printed paper, ink-on-substrate systems, and stacked transparencies—application domains where KM theory is known to work well.

The Hébert–Hersch framework operates at the level of the KM quantities themselves: the phase function  $p(\mu, \mu')$ , the asymmetry parameter  $g$ , and the distinction between forward-peaked and isotropic scattering do not appear in the compositional algebra, nor do they need to in those application domains. This raises a question that is not immediately obvious: why should a rank-2 model—one that cannot distinguish  $g = 0.90$  from  $g = 0.99$ —succeed so consistently in predicting color-accurate reflectance for real printed systems? The present paper addresses the logically prior question that the compositional approach takes as given: what, exactly, is the relationship between the full angular transport problem and the two-flux description? Where does the phase function enter? Where does it get lost? And why does the transfer-matrix algebra work so well?

A useful way to situate Kubelka–Munk theory within the broader family of transport approximations is to recognize that many classical models arise from different projections of the same radiative transfer operator onto different angular subspaces. In the present formulation, the two-flux Kubelka–Munk equations correspond to a projection onto the hemispherical subspace spanned by the indicator functions  $\{\chi^+, \chi^-\}$ , which retain only the directional sign of the radiance (forward versus backward) while discarding all finer angular structure. By contrast, the diffusion or  $P_1$  approximation projects onto the Legendre subspace  $\{1, \mu\}$ , preserving the first angular moment and therefore the angular gradient of the intensity. Discrete ordinates methods ( $S_N$ ) can likewise be interpreted as projections onto a set of directional delta functions representing selected propagation angles. From this viewpoint these methods are not competing theories but different low-dimensional reductions of the same infinite-dimensional transport problem, each retaining different angular information. Kubelka–Munk sits at the extreme end of this hierarchy: it preserves geometric directionality (forward versus backward flux) while discarding all internal angular resolution within each hemisphere. Understanding KM theory in this projection framework clarifies both its remarkable practical success in multiply scattering media and its intrinsic limitations in strongly anisotropic or optically thin regimes.

We show that the KM equations arise exactly as a rank-2 Galerkin projection of the full radiative transfer equation onto the subspace spanned by hemispherical characteristic functions. This is not just a formal observation. It tells us what KM theory can and cannot represent, why multilayer composition preserves angular rank, and where the boundary lies between media for which the

two-flux description is adequate and those for which it is not.

Throughout, we work in the steady-state, plane-parallel, azimuthally-symmetric setting with no emission.

## 2 The radiative transfer equation

The starting point is the steady-state, plane-parallel radiative transfer equation [15] for the specific intensity  $I(z, \mu)$ :

$$\mu \frac{\partial I}{\partial z} = -(\sigma_a + \sigma_s) I + \frac{\sigma_s}{2} \int_{-1}^1 p(\mu, \mu') I(z, \mu') d\mu', \quad (1)$$

where  $z$  is depth along the slab normal,  $\mu = \cos \theta$  is the direction cosine,  $\sigma_a$  and  $\sigma_s$  are the absorption and scattering coefficients, and  $p(\mu, \mu')$  is the phase function, normalized so that  $\int_{-1}^1 p(\mu, \mu') d\mu' = 2$  for each  $\mu$ . (Some authors normalize to unity or to  $4\pi$ ; only numerical prefactors change.)

The key feature of this equation is that it is infinite-dimensional in angle. At every depth  $z$ , the unknown is not a number or a pair of numbers but a function on  $[-1, 1]$ . Any practical method of solution must reduce this to something finite. Different reduction strategies—spherical harmonics, discrete ordinates, Monte Carlo, two-flux averaging—define different families of approximate transport theories. The question is where KM theory sits in this landscape.

## 3 Functional setting

We need a small amount of notation. Let  $\mathcal{H} = L^2([-1, 1])$  be the space of square-integrable functions on the angular domain, with the standard inner product  $\langle f, g \rangle = \int_{-1}^1 f(\mu) g(\mu) d\mu$ .

The transport operator acts on  $I(z, \cdot) \in \mathcal{H}$  as

$$\mathcal{T}[I] = \mu \partial_z I + (\sigma_a + \sigma_s) I - \frac{\sigma_s}{2} \mathcal{K}_p[I], \quad (2)$$

where  $\mathcal{K}_p$  is the integral scattering operator:  $(\mathcal{K}_p[I])(\mu) = \int_{-1}^1 p(\mu, \mu') I(\mu') d\mu'$ . Since  $\mathcal{H}$  is infinite-dimensional, so is the state space of the RTE. Any finite-dimensional approximation amounts to choosing a subspace  $V \subset \mathcal{H}$  and projecting the physics onto it. The character of the approximation—what it captures and what it loses—is determined entirely by the choice of  $V$ .

*Remark on rigor.* We treat  $\mathcal{T}$  formally as an unbounded operator on  $\mathcal{H}$ ; all manipulations below (projections, inner products, term-by-term integration) can be justified for smooth, compactly supported test functions and extended by density to  $L^2$ . We will not belabor domain questions, since the projection itself maps to a finite-dimensional subspace on which all operators are bounded.

## 4 Comparison: the diffusion ( $P_1$ ) approximation

Before getting to KM, it helps to recall the diffusion approximation, because it is also two-dimensional and often confused with KM theory. As we will show in Section 6, KM theory projects onto the hemispherical subspace  $\text{span}\{\chi^+, \chi^-\}$ ; diffusion theory projects onto a different two-dimensional subspace.

The  $P_1$  approximation expands the intensity in the first two Legendre polynomials:

$$I(z, \mu) \approx \frac{1}{2} \phi(z) + \frac{3}{2} \mu J(z), \quad (3)$$

Table 1: Summary of notation for hemispherical phase-function integrals and derived quantities.

Symbol	Meaning
$\chi^+, \chi^-$	Forward/backward hemispherical indicator functions
$\mathcal{P}$	Hemispherical projection operator
$\bar{p}_{++}$	$\int_0^1 \int_0^1 p(\mu, \mu') d\mu' d\mu$ (forward-to-forward)
$\bar{p}_{-+}$	$\int_0^1 \int_{-1}^0 p(\mu, \mu') d\mu' d\mu$ (backscatter fraction)
$K = 2\sigma_a$	KM absorption coefficient
$S = \sigma_s \bar{p}_{-+}$	KM scattering coefficient
$g = \frac{1}{2} \int_{-1}^1 \mu p(\mu) d\mu$	Asymmetry parameter (invisible to $\mathcal{P}$ )
$\varepsilon = \ I^{(\perp)}\ /\ I\ $	Relative projection error
$\tau^* = \tau(1 - g)$	Reduced optical thickness
$\gamma = \sqrt{K(K + 2S)}$	KM eigenvalue parameter

where  $\phi$  is the scalar fluence and  $J$  is the net current. Scattering anisotropy enters through the reduced scattering coefficient  $\sigma_s^* = \sigma_s(1 - g)$ , where  $g = \frac{1}{2} \int_{-1}^1 \mu p(\mu) d\mu$  is the asymmetry parameter. The underlying subspace is  $V_{P_1} = \text{span}\{1, \mu\}$ : diffusion theory retains the first angular moment of the phase function and captures angular gradient structure through the  $\mu$  component.

KM theory, as we will see, uses a different two-dimensional subspace that captures angular *sign* structure—forward versus backward—but no gradient. Same rank, completely different physics. The two approximations are complementary, not equivalent. Consider Henyey–Greenstein scattering with  $g = 0.95$ : diffusion theory sees  $g$  through  $\sigma_s^* = \sigma_s(1 - g)$  and correctly identifies the slab as transport-thin. KM theory sees only  $\bar{p}_{-+}$  and cannot distinguish  $g = 0.90$  from  $g = 0.99$  when their backscatter fractions are similar—precisely the regime where the distinction matters most.

## 5 The hemispherical projection

Now we get to the heart of the matter. Define two hemispherical indicator functions:

$$\chi^+(\mu) = \begin{cases} 1, & \mu > 0, \\ 0, & \mu \leq 0, \end{cases} \quad \chi^-(\mu) = \begin{cases} 0, & \mu \geq 0, \\ 1, & \mu < 0. \end{cases} \quad (4)$$

These are orthogonal ( $\langle \chi^+, \chi^- \rangle = 0$ ) and normalized ( $\langle \chi^+, \chi^+ \rangle = \langle \chi^-, \chi^- \rangle = 1$ ).

The projection operator  $\mathcal{P}$  maps any angular distribution to its hemispherical averages:

$$\mathcal{P}f = \langle f, \chi^+ \rangle \chi^+ + \langle f, \chi^- \rangle \chi^-. \quad (5)$$

In plain language: replace  $f(\mu)$  for all  $\mu > 0$  by its average over the forward hemisphere, and replace  $f(\mu)$  for all  $\mu < 0$  by its average over the backward hemisphere.

Three properties matter. First,  $\mathcal{P}^2 = \mathcal{P}$  (idempotence)—projecting twice is the same as projecting once. Second,  $\mathcal{P}$  is self-adjoint with respect to the flat  $L^2$  inner product  $\langle f, g \rangle = \int f g d\mu$ . Third, the range of  $\mathcal{P}$  is two-dimensional:  $\text{range}(\mathcal{P}) = \text{span}\{\chi^+, \chi^-\}$ .

This is the coarsest angular discretization that preserves the distinction between forward and backward. It respects the slab geometry—light going left versus light going right—but resolves nothing finer than that within either hemisphere. That is what gives KM theory its characteristic combination of geometric realism and angular coarseness.

*Remark on the inner product.* The flat  $L^2$  measure  $\langle f, g \rangle = \int f g d\mu$  is the natural choice for projecting the integral scattering operator, since all directions within a hemisphere contribute equally to the hemispherical flux. Under the transport-weighted measure  $\langle f, g \rangle_\mu = \int |\mu| f g d\mu$ —which makes the streaming operator self-adjoint—the hemispherical basis functions are not orthogonal, and  $\mathcal{P}$  would not be an orthogonal projection. The flat-measure projection minimizes the  $L^2([-1, 1])$  norm of the residual, not the flux-weighted norm; the two criteria differ most for grazing angles ( $\mu \rightarrow 0$ ), which contribute little to net flux but equally to the flat-measure error. In practice, the distinction is secondary for optically thick media where the angular distribution is already nearly flat within each hemisphere.

## 6 The central result: KM as projected transport

**Main result.** The Kubelka–Munk transport operator is exactly the rank-2 Galerkin projection of the radiative transfer operator onto the hemispherical subspace  $\text{span}\{\chi^+, \chi^-\}$ :

$$\mathcal{T}_{\text{KM}} = \mathcal{P} \mathcal{T} \mathcal{P}.$$

The KM coefficients are  $K = 2\sigma_a$  and  $S = \sigma_s \bar{p}_{-+}$ , where  $\bar{p}_{-+}$  is the hemispherical backscatter fraction of the phase function. The projection is idempotent ( $\mathcal{P}^2 = \mathcal{P}$ ), its kernel is infinite-dimensional, and its rank is preserved under multilayer composition.

The claim is that the KM operator is exactly the “sandwich”

$$\mathcal{T}_{\text{KM}} = \mathcal{P} \mathcal{T} \mathcal{P}. \quad (6)$$

That is: restrict the intensity to the hemispherical subspace, apply the full transport operator, then project back.

We now carry out this projection in full. Write the projected intensity as

$$(\mathcal{P}I)(z, \mu) = I^+(z) \chi^+(\mu) + I^-(z) \chi^-(\mu), \quad (7)$$

where the hemispherical fluxes are

$$I^+ = \int_0^1 I d\mu, \quad I^- = \int_{-1}^0 I d\mu.$$

### Step 1: The streaming term

Apply the streaming part of  $\mathcal{T}$  to the projected intensity and take the inner product with  $\chi^+$ :

$$\langle \mu \partial_z (\mathcal{P}I), \chi^+ \rangle = \frac{dI^+}{dz} \int_0^1 \mu d\mu = \frac{1}{2} \frac{dI^+}{dz}. \quad (8)$$

For the backward hemisphere, the same computation gives  $\langle \mu \partial_z (\mathcal{P}I), \chi^- \rangle = \frac{1}{2} \frac{dI^-}{dz}$  (with  $\int_{-1}^0 \mu d\mu = -\frac{1}{2}$ , the sign being absorbed into the direction of  $I^-$ ). The factor  $\frac{1}{2}$  from  $\int_0^1 \mu d\mu$  is the origin of the classical factor-of-2 relationship between KM and transport coefficients discussed many times in the literature [13]; here it emerges from the projection.

## Step 2: The extinction term

The extinction (absorption plus out-scattering) contribution is

$$\langle (\sigma_a + \sigma_s) \mathcal{P}I, \chi^+ \rangle = (\sigma_a + \sigma_s) I^+ \underbrace{\langle \chi^+, \chi^+ \rangle}_{=1} = (\sigma_a + \sigma_s) I^+. \quad (9)$$

## Step 3: The scattering integral

This is where the phase function enters—and where it gets averaged away. Apply  $\mathcal{K}_p$  to the projected intensity and project onto  $\chi^+$ :

$$\begin{aligned} \langle \mathcal{K}_p[\mathcal{P}I], \chi^+ \rangle &= \int_0^1 \int_{-1}^1 p(\mu, \mu') [I^+ \chi^+(\mu') + I^- \chi^-(\mu')] d\mu' d\mu \\ &= I^+ \underbrace{\int_0^1 \int_0^1 p(\mu, \mu') d\mu' d\mu}_{\equiv \bar{p}_{++}} + I^- \underbrace{\int_0^1 \int_{-1}^0 p(\mu, \mu') d\mu' d\mu}_{\equiv \bar{p}_{-+}}. \end{aligned} \quad (10)$$

Here  $\bar{p}_{++}$  is the forward-to-forward hemispherical average of the phase function (light staying in the forward hemisphere), and  $\bar{p}_{-+}$  is the backward-to-forward average (light scattered from backward into forward). The phase-function normalization  $\int_{-1}^1 p(\mu, \mu') d\mu' = 2$  for each  $\mu$  gives

$$\bar{p}_{++} + \bar{p}_{-+} = \int_0^1 \int_{-1}^1 p d\mu' d\mu = 2. \quad (11)$$

By the symmetry  $p(\mu, \mu') = p(-\mu, -\mu')$  of the azimuthally-averaged phase function in slab geometry, the backward-hemisphere equation involves the same two integrals:  $\bar{p}_{--} = \bar{p}_{++}$  and  $\bar{p}_{+-} = \bar{p}_{-+}$ .

## Step 4: Assembling the KM equations

Combining Steps 1–3 and requiring that the residual be orthogonal to  $\text{range}(\mathcal{P})$ —the Galerkin condition—we obtain for the forward flux:

$$\frac{1}{2} \frac{dI^+}{dz} = -(\sigma_a + \sigma_s) I^+ + \frac{\sigma_s}{2} (\bar{p}_{++} I^+ + \bar{p}_{-+} I^-). \quad (12)$$

Multiply through by 2 and collect terms using  $\bar{p}_{++} = 2 - \bar{p}_{-+}$  from Eq. (11):

$$\begin{aligned} \frac{dI^+}{dz} &= -2(\sigma_a + \sigma_s) I^+ + \sigma_s(2 - \bar{p}_{-+}) I^+ + \sigma_s \bar{p}_{-+} I^- \\ &= -[2\sigma_a + 2\sigma_s - \sigma_s(2 - \bar{p}_{-+})] I^+ + \sigma_s \bar{p}_{-+} I^- \\ &= -(2\sigma_a + \sigma_s \bar{p}_{-+}) I^+ + \sigma_s \bar{p}_{-+} I^-. \end{aligned} \quad (13)$$

In the last line, the  $2\sigma_s$  from extinction and the  $2\sigma_s$  from forward in-scattering cancel, leaving only absorption and backscatter. Defining the KM coefficients

$$\boxed{K = 2\sigma_a, \quad S = \sigma_s \bar{p}_{-+}}, \quad (14)$$

where  $\bar{p}_{-+} = \int_0^1 \int_{-1}^0 p(\mu, \mu') d\mu' d\mu$  is the hemispherical backscatter fraction, Eq. (13) becomes

$$\frac{dI^+}{dz} = -(K + S) I^+ + S I^-. \quad (15)$$

An identical computation for the backward hemisphere (projecting onto  $\chi^-$ ) yields

$$\frac{dI^-}{dz} = (K + S)I^- - SI^+. \quad (16)$$

Equations (15)–(16) are the Kubelka–Munk equations. They have been derived here by pure linear algebra—an orthogonal projection of the full transport operator onto the hemispherical subspace  $\text{span}\{\chi^+, \chi^-\}$ —with no additional physical approximations beyond the projection itself. The choice of subspace *is* the approximation; every other step is exact. Because  $\mathcal{P}^2 = \mathcal{P}$ , the operator  $\mathcal{P}\mathcal{T}\mathcal{P}$  is a genuine Galerkin projection: it maps the two-dimensional range( $\mathcal{P}$ ) to itself. (The projection is Galerkin in the sense that the trial and test spaces coincide; the underlying transport operator is non-self-adjoint and no variational principle is invoked. The hemispherical basis functions are piecewise constant—degree-zero discontinuous elements on  $[-1, 0]$  and  $[0, 1]$ —making this the lowest-order discontinuous Galerkin discretization of the angular variable.)

## 7 What the projection throws away

The kernel of  $\mathcal{P}$  consists of all functions whose hemispherical averages vanish:

$$\ker(\mathcal{P}) = \left\{ f \in L^2([-1, 1]) : \int_0^1 f \, d\mu = 0 \text{ and } \int_{-1}^0 f \, d\mu = 0 \right\}. \quad (17)$$

This is infinite-dimensional. It contains every angular variation within a hemisphere: any forward-peaked structure, any oscillatory detail, any departure from a flat distribution—as long as it averages to zero over the hemisphere. Two phase functions that produce the same hemispherical backscatter fraction  $\bar{p}_{-+}$  but have wildly different angular profiles are mapped to the same KM parameters.

This is the rigorous version of what practitioners in color science and coatings—the primary users of KM theory—have always known intuitively: KM theory “cannot see” angular detail. But the projection framework makes it precise. It is not that KM theory is a poor approximation; it is an exact projection that discards a specific, identifiable, infinite-dimensional piece of the angular distribution. The discarded piece has a name— $\ker(\mathcal{P})$ —and everything we need to know about when KM theory will work well and when it will not comes down to how much energy the true solution carries in that kernel.

For instance, the function  $f(\mu) = \mu - \frac{1}{2}$  on  $[0, 1]$  (extended antisymmetrically to  $[-1, 0]$ ) has zero hemispherical average on each half—it belongs to  $\ker(\mathcal{P})$ —yet it carries the linear angular gradient that distinguishes a forward-peaked distribution from an isotropic one.

## 8 How this differs from discrete ordinates ( $S_2$ )

The two-point discrete-ordinates method ( $S_2$ ) also produces a pair of coupled ODEs that look a lot like the KM equations. It selects two directions  $\pm\mu_0$  (typically  $\mu_0 = 1/\sqrt{3}$ ) and evaluates the RTE at those specific angles.

Despite the algebraic resemblance, the methods are structurally different.  $S_2$  is a collocation method: it demands that the equation hold exactly at selected points and samples the phase function at specific angle pairs. KM theory is a Galerkin method: it integrates the equation over hemispheres, averaging the phase function rather than sampling it. The quadrature weight in KM is unity over each hemisphere (all directions contribute equally); in  $S_2$  it is effectively a Dirac delta at  $\pm\mu_0$ .

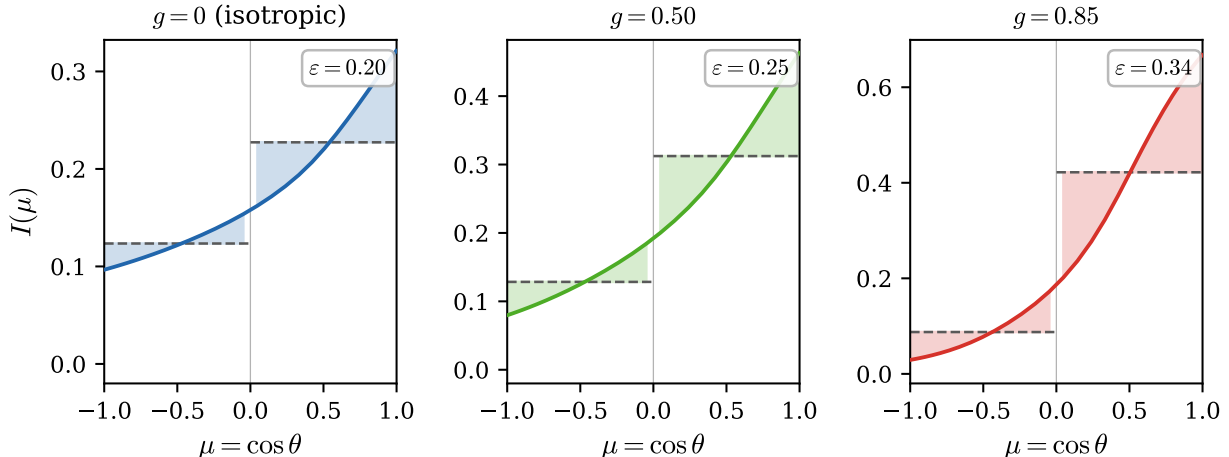


Figure 1: Angular intensity  $I(\mu)$  at the slab midplane ( $\tau = 5$ ,  $\omega = 0.9$ ) for three scattering regimes (32-stream discrete-ordinates reference solution). Dashed lines: hemispherical projection  $\mathcal{P}I$ ; shaded regions: kernel component  $I^{(\perp)} = I - \mathcal{P}I$ . The projection error  $\varepsilon$  grows from 0.20 (isotropic) to 0.34 ( $g = 0.85$ ).

The two methods respond differently to anisotropy.  $S_2$  retains directional information at the selected ordinate; KM averages it out. They coincide only for isotropic scattering, where the distinction between sampling and averaging disappears.

A small numerical example makes the divergence concrete. For the standard slab ( $\tau = 5$ ,  $\omega = 0.9$ ) with isotropic scattering, the  $S_{32}$  reference reflectance is  $R = 0.518$ ; KM gives 0.519 and  $S_2$  gives 0.518—all three agree. At  $g = 0.50$ , KM gives  $R = 0.434$  (an error of 0.021 against the reference) while  $S_2$  gives  $R = 0.591$  (error 0.179). The  $S_2$  error is nearly ten times larger, because the forward peak evaluated at  $\mu_0 = 1/\sqrt{3}$  distorts the point-sampled phase function. KM theory, by averaging over the hemisphere, is less sensitive to the shape of the forward peak—which is both its limitation and, in this case, its advantage.

## 9 Forward-peaked scattering and the loss of $g$

The limitations of the hemispherical projection are most acute for strongly forward-peaked scattering. For Henyey–Greenstein scattering with asymmetry parameter  $g$ , the transport mean free path is

$$\ell^* = \frac{\ell}{1 - g}, \quad (18)$$

where  $\ell = 1/(\sigma_a + \sigma_s)$ . As  $g \rightarrow 1$ , the phase function concentrates into a narrow forward peak. The energy in this peak lies entirely within  $\ker(\mathcal{P})$ : it is angular structure within the forward hemisphere that averages to zero against the flat basis function  $\chi^+$ . The projected operator  $\mathcal{P}T\mathcal{P}$  sees only the total backscatter fraction and is blind to the shape of the forward peak.

KM theory is therefore insensitive to the distinction between, say,  $g = 0.9$  and  $g = 0.99$  whenever the backscatter fractions are similar. All the angular structure that separates these two very different scattering regimes resides in  $\ker(\mathcal{P})$ . This insensitivity is intrinsic to the hemispherical projection and therefore propagates to any formalism that operates within the projected subspace, including the compositional models of Hébert and Hersch [5]. In the application domains where those models

have been validated—printed paper, ink-on-substrate systems—this is not a limitation in practice, because multiple scattering in the substrate has already isotropized the angular distribution. The information about  $g$  has been erased by the physics, not by the model. In forward-peaked media, however, this information is physically present and its loss is consequential.

Corrections such as the  $\delta$ -Eddington [16] and  $\delta$ - $M$  [17] methods can be understood precisely in this framework. The  $\delta$ - $M$  method replaces the phase function by

$$p(\mu, \mu') \longrightarrow (1 - f) p^*(\mu, \mu') + 2f \delta(\mu - \mu'),$$

where  $f = g^N$  is the forward-peak fraction and  $p^*$  is a smoother residual phase function. The  $\delta$ -function term, being perfectly forward-peaked, has zero hemispherical backscatter and therefore lies entirely in  $\ker(\mathcal{P})$ . The  $\delta$ - $M$  truncation removes this component *before* projecting, transferring its energy into a renormalized extinction coefficient. In projection-theoretic language, the modified transport problem has a solution whose kernel component  $\|I^{(\perp)}\|$  is smaller, thereby reducing  $\varepsilon$ . The procedure does not enlarge the projected subspace—KM theory still operates in rank 2—but it ensures that the solution being projected has less energy in the piece the projection discards. The connection between forward-peak asymptotics and the Cauchy kernel structure of the Henyey–Greenstein phase function is developed in [3]: when expanded on the Motzkin polynomial basis, the Henyey–Greenstein phase function exhibits Cauchy/Lorentzian kernel asymptotics in the  $g \rightarrow 1$  limit, providing an independent characterization of the angular information that the hemispherical projection discards.

## 10 The thin-slab regime

In optically thin media ( $\sigma_t L \ll 1$ ), the intensity is dominated by the ballistic (unscattered) component, which decays as  $\exp(-\sigma_t z/\mu)$ . This signal is sharply directional—it remembers the angle of incidence—and a hemispherical average misrepresents it badly.

A quantitative estimate is straightforward. For diffuse illumination ( $I = 1$  for  $\mu > 0$  at the top surface), the ballistic contribution at optical depth  $t$  is  $I_{\text{ball}}(\mu) = e^{-t/\mu}$  on the forward hemisphere. The hemispherical average of this signal is the second exponential integral,  $\langle I_{\text{ball}}, \chi^+ \rangle = E_2(t)$ , and the  $L^2$  norm satisfies  $\|I_{\text{ball}}\|^2 = E_2(2t)$ . The projection error on the forward hemisphere alone is therefore

$$\varepsilon_{\text{ball}}(t) = \sqrt{1 - \frac{E_2(t)^2}{E_2(2t)}}. \quad (19)$$

For  $t = 0.5$  (the midplane of a slab with  $\tau = 1$ ), this gives  $\varepsilon_{\text{ball}} \approx 0.53$ ; for  $t = 2.5$  (midplane of  $\tau = 5$ ),  $\varepsilon_{\text{ball}} \approx 0.78$ . The ballistic estimate serves as a heuristic upper bound on the actual projection error: multiple scattering tends to isotropize the distribution and pull it toward  $\text{range}(\mathcal{P})$ , so the fully scattered solution generally has smaller  $\varepsilon$  than the unscattered one. The numerical solutions in Section 12 confirm that the true  $\varepsilon_{\text{mid}}$  is considerably smaller once scattering is included, though a rigorous proof that multiple scattering always reduces the projection error is not attempted here. But Eq. (19) establishes that  $\varepsilon \rightarrow O(1)$  for optically thin slabs, confirming that the two-flux description is unreliable in that regime.

Conversely, in optically thick media ( $\sigma_t L \gg 1$ ), multiple scattering randomizes the angular distribution within each hemisphere. The true intensity moves toward  $\text{range}(\mathcal{P})$ , the projection error shrinks, and KM theory becomes increasingly faithful. This is a general property of projection methods: they work best when the true solution already lives near the subspace you are projecting onto.

## 11 Projection error and applicability

The previous two sections point to a general principle. At each depth  $z$ , the true intensity decomposes as  $I = \mathcal{P}I + I^{(\perp)}$ , where  $I^{(\perp)} \in \ker(\mathcal{P})$  is the component the projection throws away. The relative projection error,

$$\varepsilon(z) = \frac{\|I^{(\perp)}(z, \cdot)\|}{\|I(z, \cdot)\|}, \quad (20)$$

is the natural figure of merit. When  $\varepsilon$  is small, KM theory is accurate. When it is not, no amount of algebraic sophistication in the compositional framework can compensate, because the information has already been lost at the projection step.

**Where KM works well.** Optically thick, multiply scattering media with moderate anisotropy—paper, paint films, coatings, textile layers. After many scattering events the angular distribution within each hemisphere is nearly flat, so  $\|I^{(\perp)}\|$  is small and the hemispherical averages capture almost everything.

This is the domain in which the compositional models of Hébert and Hersch [4, 5, 6] achieve their impressive accuracy (typical color differences  $\Delta E_{94}^* < 1$ ). The key mechanism is that the physics of multiple scattering isotropizes the angular distribution *before* the KM projection acts on it—the information about  $g$  and the shape of the forward peak has already been destroyed by the medium, not by the model. Paper substrates are heavily scattering: by the time light has bounced through a mat of cellulose fibers, the angular distribution within each hemisphere is nearly flat and  $\|I^{(\perp)}\|$  is genuinely small. Ink layers attenuate primarily by Beer–Lambert absorption—there is almost no scattering to have a phase function of. Interfaces are handled by Fresnel coefficients—exact geometric optics and angular-rank-preserving by the argument of Section 14. The excellent accuracy reported for these systems is real and well-earned; the projection-error framework explains *why*.

Even within the paper domain, the projection is not perfect. Edström [14], comparing KM against the discrete-ordinates solver DORT2002, found that KM reflectance errors can reach 20% for strongly absorbing papers. Strong absorption reduces the number of scattering events needed to isotropize the angular distribution, leaving more energy in  $\ker(\mathcal{P})$ —exactly what the projection-error framework predicts.

**Where KM breaks down.** Biological tissue ( $g \approx 0.95$ ), atmospheric aerosols, sea water, clouds—any medium where the phase function has a strong forward peak. The peak energy lives in  $\ker(\mathcal{P})$ , the projection error is large, and the KM scattering coefficient  $S$  cannot distinguish qualitatively different scattering regimes. This is not a deficiency of any particular implementation; it is a structural consequence of the rank-2 projection. Higher-order methods— $P_N$ ,  $S_N$ , Monte Carlo—are essential.

**Thin slabs.** The ballistic component dominates,  $\varepsilon \rightarrow O(1)$ , and the measured reflectance and transmittance depend on the angular distribution of the illumination—something the two-flux framework does not track.

The projection-error criterion unifies these observations. KM theory succeeds when multiple scattering has driven the angular distribution toward  $\text{range}(\mathcal{P})$ , and it fails when significant energy remains in  $\ker(\mathcal{P})$ . The accuracy of any model that takes KM parameters as inputs is bounded by the same criterion.

Table 2: Projection error and reflectance/transmittance comparison for three scattering regimes at  $\tau = 5$ ,  $\omega = 0.9$ .  $R$  and  $T$  are hemispherical reflectance and transmittance; subscripts denote the  $S_{32}$  reference and KM solutions.  $\varepsilon_{\text{mid}}$  is the projection error at the slab midplane;  $\varepsilon_{\text{max}}$  is the maximum over the slab.

$g$	$\tau^*$	$R_{\text{SN}}$	$R_{\text{KM}}$	$T_{\text{SN}}$	$T_{\text{KM}}$	$ \Delta R $	$\varepsilon_{\text{mid}}$	$\varepsilon_{\text{max}}$
0.00	5.00	0.518	0.519	0.044	0.031	0.001	0.20	0.33
0.50	2.50	0.413	0.434	0.099	0.064	0.021	0.25	0.35
0.85	0.75	0.239	0.285	0.212	0.148	0.046	0.34	0.42

## 12 Numerical illustration

To make the projection-error framework concrete, we compute  $\varepsilon$  for three representative cases: isotropic scattering ( $g = 0$ ), moderate anisotropy ( $g = 0.50$ ), and strongly forward-peaked scattering ( $g = 0.85$ ), all at total optical thickness  $\tau = 5$  and single-scattering albedo  $\omega = 0.9$ . The boundary conditions are diffuse illumination from above ( $I(0, \mu) = 1$  for  $\mu > 0$ ) and no light from below.

The reference solution is computed by an  $S_{32}$  discrete-ordinates solver with Gauss–Legendre quadrature. The solution is well converged: results change by less than  $10^{-4}$  in reflectance at  $S_{64}$ , and the 32-term Legendre expansion of the phase function is more than adequate for  $g \leq 0.85$ . The KM solution is computed directly from Eqs. (15)–(16) with  $K$  and  $S$  given by Eq. (14) using the numerically evaluated hemispherical phase-function integrals.

Table 2 and Fig. 3 display the results. The three cases share the same total optical depth  $\tau = 5$ , but the *reduced* optical depths  $\tau^* = \tau(1 - g)$  range from 5.0 (isotropic) to 0.75 ( $g = 0.85$ ). In transport terms, the  $g = 0.85$  slab is optically thin despite having the same  $\tau$ —and the projection error reflects this. Thus  $\tau^*$  is the natural dimensionless control parameter governing KM accuracy: the two-flux description is reliable when  $\tau^* \gg 1$ , even if  $\tau$  itself is modest.

To test this more broadly, Fig. 2 shows  $\varepsilon_{\text{mid}}$  as a function of  $\tau^*$  for a range of  $\tau$  (2, 5, 10, 20),  $g$  (0–0.85), and two values of  $\omega$  (0.7 and 0.9). The curves do not collapse perfectly— $\omega$  shifts the baseline, since lower albedo means fewer scattering events and therefore less isotropization—but within each albedo family,  $\tau^*$  organizes the data far better than either  $\tau$  or  $g$  alone. All points with  $\tau^* > 5$  have  $\varepsilon_{\text{mid}} < 0.25$ ; all points with  $\tau^* < 1$  exceed 0.30. This confirms that  $\tau^*$  is the right control parameter, with  $\omega$  as a secondary factor.

Two features are noteworthy. First, the midplane projection error  $\varepsilon_{\text{mid}}$  tracks  $g$  monotonically: 0.20 for isotropic, 0.25 for  $g = 0.50$ , and 0.34 for  $g = 0.85$ . This is exactly what the kernel analysis of Section 7 predicts: more forward-peaked scattering means more energy in  $\ker(\mathcal{P})$ .

Second, the reflectance error  $|\Delta R|$  is much smaller than  $\varepsilon$  in every case. For isotropic scattering,  $\varepsilon_{\text{mid}} = 0.20$  but  $|\Delta R| = 0.001$ . This is because hemispherical reflectance is itself a projected quantity—it is  $\langle I^-, \chi^- \rangle$  evaluated at the boundary—and is therefore partially buffered from the angular errors that  $\varepsilon$  measures. The projection error bounds the observable error but does not saturate it. This is the numerical confirmation of the mechanism identified in Section 11: in multiply scattering media the hemispherical observables are precisely the quantities the projection *does* capture, which is why the Hébert–Hersch compositional models achieve the color accuracy they do even though the underlying two-flux approximation is coarse.

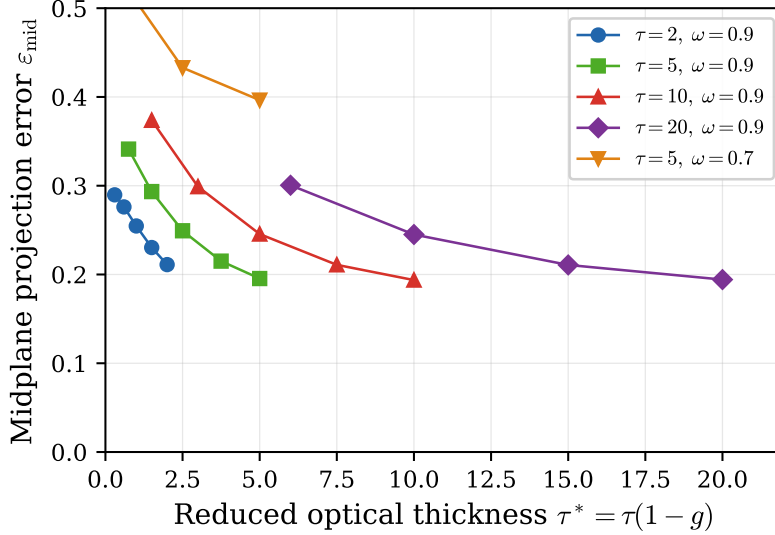


Figure 2: Midplane projection error  $\varepsilon_{\text{mid}}$  versus reduced optical thickness  $\tau^* = \tau(1 - g)$  for a range of slab parameters. Within each albedo family,  $\tau^*$  organizes the data: slabs with  $\tau^* \gg 1$  are well described by KM theory regardless of the individual values of  $\tau$  and  $g$ .

### 13 Multilayer transfer matrices

For a homogeneous layer of thickness  $d$  with KM parameters  $(K, S)$ , define

$$\gamma = \sqrt{K(K + 2S)}. \quad (21)$$

The KM equations (15)–(16) have a matrix solution:

$$\begin{pmatrix} I^+(d) \\ I^-(d) \end{pmatrix} = M(d) \begin{pmatrix} I^+(0) \\ I^-(0) \end{pmatrix}, \quad (22)$$

where

$$M(d) = \begin{pmatrix} \cosh(\gamma d) + \frac{K + S}{\gamma} \sinh(\gamma d) & \frac{S}{\gamma} \sinh(\gamma d) \\ -\frac{S}{\gamma} \sinh(\gamma d) & \cosh(\gamma d) - \frac{K + S}{\gamma} \sinh(\gamma d) \end{pmatrix}. \quad (23)$$

Stacking  $n$  layers with parameters  $(K_i, S_i, d_i)$  gives

$$M_{\text{total}} = M_n(d_n) \cdots M_2(d_2) M_1(d_1). \quad (24)$$

Each factor is  $2 \times 2$ , and so is the product. The entire multilayer calculation lives within the two-dimensional projected space.

This matrix-multiplicative structure is the algebraic machinery exploited in the compositional models of Hébert and Hersch [5, 6], who showed that layer composition via transfer matrices unifies Kubelka’s layering formulae, the Saunderson correction, and the Williams–Clapper model. Their approach works directly with the layer matrices, composing them without needing to revisit the transport equation for each layer. The present analysis reveals the operator-theoretic origin of these matrices: they are the natural representation of the transport operator restricted to  $\text{range}(\mathcal{P})$ . This is why the formalism works so cleanly—it is not an approximation to the transfer matrix; it is the transfer matrix of the projected problem.

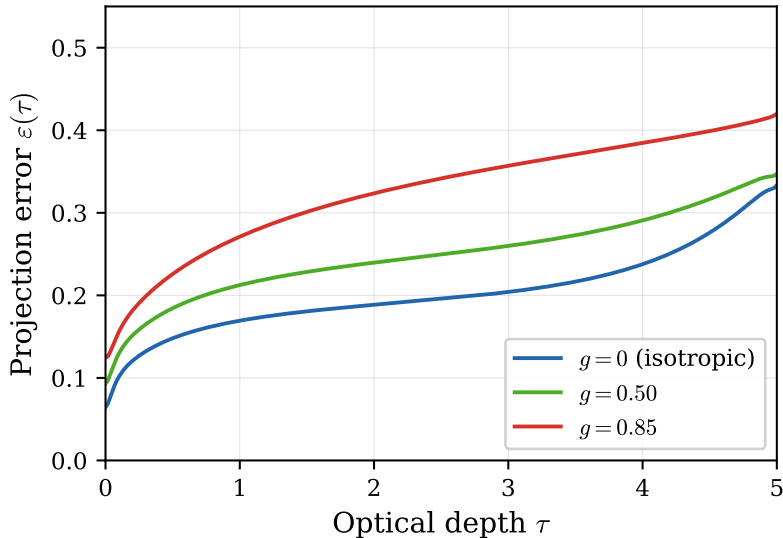


Figure 3: Projection error  $\varepsilon(\tau)$  through the slab ( $\tau = 5$ ,  $\omega = 0.9$ ) for three values of  $g$ . The error is smallest at the illuminated face and grows toward the exit; higher  $g$  gives higher  $\varepsilon$  at every depth.

## 14 Rank preservation

Since  $\text{range}(\mathcal{P})$  is two-dimensional, every projected layer operator maps this subspace to itself. Composing  $n$  such operators gives a map from a two-dimensional space to a two-dimensional space, which has rank at most 2 regardless of  $n$ . In the matrix language: every  $M_i$  is  $2 \times 2$ , and so is their product.

**Proposition 1** (Rank preservation). *Let  $\mathcal{P}$  be the hemispherical projection of rank 2. For any sequence of projected layer operators  $M_1, \dots, M_n$  acting on  $\text{range}(\mathcal{P})$ , the composite operator  $M_{\text{total}} = M_n \cdots M_1$  has rank at most 2. No multilayer composition can recover angular information annihilated by  $\mathcal{P}$ .*

The physical consequence is important and sometimes overlooked: stacking many KM layers does not improve the angular resolution. A 100-layer calculation has the same angular resolution—none within each hemisphere—as a single-layer calculation. More layers give you more spectral or spatial detail, but the same two-dimensional angular view.

Improving angular resolution requires enlarging the projected subspace, i.e., going to a higher-order method. The four-flux matrix models developed by Simonot et al. [8] and the multiflux extensions described by Hébert [7] do exactly this: they enlarge the subspace to dimension 4 (separating collimated from diffuse components in each hemisphere) while preserving the transfer-matrix formalism. In the language of this paper, they replace  $\mathcal{P}$  with a higher-rank projector.

*Remark on interfaces.* Fresnel boundary conditions do not increase the angular rank. A planar dielectric interface reflects a fraction  $r$  of the backward flux and transmits  $(1 - r)$  of the forward flux; in the hemispherical framework this amounts to multiplying  $I^+$  and  $I^-$  by scalar Fresnel coefficients (averaged over the hemisphere). The interface matrix is therefore  $2 \times 2$  and diagonal, and its product with any KM layer matrix remains  $2 \times 2$ . Interfaces redistribute energy between the two hemispherical channels but do not create angular structure within either hemisphere. This is why the Saunderson correction and the Williams–Clapper interface model can be absorbed into the transfer-matrix formalism [5] without changing its rank.

## 15 Eigenstructure

The eigenvalues of the single-layer transfer matrix are  $\lambda_{\pm} = e^{\pm\gamma d}$ , where  $\gamma = \sqrt{K(K+2S)}$ . The spectral structure is two-dimensional regardless of layer thickness or the complexity of the phase function from which  $K$  and  $S$  were derived.

The two eigenmodes correspond to exponential growth and decay of the flux imbalance through the slab. These completely characterize transport within the KM framework. Higher angular modes—which would be needed to describe, for example, the angular profile of the transmitted beam—have been projected out and are inaccessible.

In the conservative limit ( $K \rightarrow 0$ , purely scattering medium),  $\gamma \rightarrow 0$  and the transfer matrix becomes linear in  $d$  rather than exponential:  $M(d) \rightarrow I + dA$ , where  $A$  is the generator. The eigenvalues  $\lambda_{\pm} = e^{\pm\gamma d}$  coalesce at unity, producing a degenerate case in which the flux imbalance propagates algebraically rather than exponentially. This is the well-known conservative KM limit in which reflectance grows linearly with optical thickness.

## 16 The inverse problem

For a composite medium of  $n$  layers, the parameter vector is  $\Theta = (K_1, S_1, \dots, K_n, S_n) \in \mathbb{R}^{2n}$ . But the measurable quantities—total reflectance  $R$  and total transmittance  $T$ —give only two constraints.

For a single layer with known thickness, this is exactly determined, and the classical KM inversion works. For two or more layers, the system is underdetermined:  $2n$  unknowns, 2 equations. You need additional measurements—individual layer properties, spectral data at multiple wavelengths, or angular-resolved measurements—to make the inverse problem well-posed.

The rank-2 limitation is structural, not a matter of measurement precision. It is a direct consequence of the projection: since the observables  $R$  and  $T$  are hemispherical integrals—inner products with  $\chi^{\pm}$ —they live in the two-dimensional  $\text{range}(\mathcal{P})$  and can determine at most two independent parameters per measurement. Put differently,  $\ker(\mathcal{P})$  is fundamentally unobservable to any detector that measures only hemispherical totals. The kernel is not hidden by noise or limited dynamic range; it is orthogonal to the measurement functionals and produces exactly zero signal in  $R$  and  $T$ .

No strategy based solely on hemispherical reflectance and transmittance can resolve more than this. Breaking the underdeterminacy requires either reaching into  $\ker(\mathcal{P})$  through angular-resolved detection (which directly probes the discarded angular structure) or increasing the number of projected constraints through spectral multiplexing—measuring  $R(\lambda)$  and  $T(\lambda)$  at multiple wavelengths under the assumption that  $K(\lambda)$  and  $S(\lambda)$  vary in a constrained way. Spectral multiplexing does not access  $\ker(\mathcal{P})$ ; it provides additional hemispherical measurements that help resolve  $K$  and  $S$  as functions of wavelength, but each measurement still lives in  $\text{range}(\mathcal{P})$ . The kernel is infinite-dimensional, so there is a great deal of angular information that hemispherical measurements simply cannot access.

## 17 Classification and conclusions

Multilayer KM theory is a rank-2 orthogonal projection of the radiative transfer equation onto the hemispherical subspace  $\text{span}\{\chi^+, \chi^-\}$ , summarized by  $\mathcal{T}_{\text{KM}} = \mathcal{P}\mathcal{T}\mathcal{P}$ . This places it in a hierarchy of angular approximations to the RTE:

Method	Subspace	Rank	Type
Kubelka–Munk	$\{\chi^+, \chi^-\}$	2	Galerkin
Diffusion ( $P_1$ )	$\{1, \mu\}$	2	Galerkin
$S_N$ discrete ordinates	$\{\delta(\mu - \mu_i)\}$	$N$	Collocation
$P_N$ spherical harmonics	$\{P_0, \dots, P_N\}$	$N + 1$	Galerkin
Full RTE	$L^2([-1, 1])$	$\infty$	Exact

KM theory sits at the bottom of the Galerkin ladder. It gets the geometry right—slab structure, layer composition, flux conservation—without resolving any angular detail within either hemisphere. The title phrase “geometric realism without angular resolution” is meant to capture this. The four-flux and multiframe models of Hébert et al. [7, 8] occupy the next rungs, distinguishing collimated from diffuse light and thereby handling interface effects (Fresnel reflections, Saunderson corrections) that the pure two-flux model cannot represent internally.

The kernel  $\ker(\mathcal{P})$  tells us exactly what is lost: all angular structure beyond the hemispherical average. Rank preservation guarantees this cannot be recovered by stacking layers. Non-injectivity explains why infinitely many microscopically different media can share the same KM parameters.

The numerical illustration of Section 12 anchors these abstract statements in computed quantities: the projection error  $\varepsilon$  increases from 0.20 to 0.34 as the asymmetry parameter increases from 0 to 0.85, while the reflectance error—being itself a hemispherical quantity—remains much smaller. The parametric sweep of Fig. 2 confirms that the reduced optical thickness  $\tau^* = \tau(1 - g)$  governs KM accuracy across a wide range of slab parameters, with single-scattering albedo as a secondary factor. The thin-slab asymptotic (Eq. 19) provides an analytical bound showing that  $\varepsilon \rightarrow O(1)$  when the ballistic component dominates.

KM theory is therefore best understood as a well-defined low-rank projection whose limitations are intrinsic, identifiable, and quantifiable. Understanding the projection lets practitioners use KM with confidence where it belongs—optically thick, multiply scattering media—and know precisely what is needed where it does not: a projection onto a higher-dimensional subspace. The compositional transfer-matrix programme of Hébert, Hersch, Simonot, and collaborators [5, 7, 8] provides the practical machinery for composing layers and interfaces at any flux order, and its demonstrated accuracy in printed media was, at first glance, surprisingly good for a rank-2 model. The projection-error framework explains, retroactively, why: in those systems the physics of multiple scattering has already isotropized the angular distribution, so the projection discards information that the medium itself has destroyed. The present paper provides the complementary theoretical foundation: the Galerkin projection identifies  $K$  and  $S$  as hemispherical moments of the transport operator, shows that  $g$  and all higher angular structure are annihilated by the projection, explains why the transfer-matrix formalism is natural for the projected problem, and shows where the two-flux description stops working.

## Acknowledgments

The author thanks Bob Cordery for ongoing discussions on radiative transport and light scattering, including the joint work on Motzkin polynomial representations [3], that motivated much of this work.

The author used Claude (Anthropic) as an AI assistant for mathematical checking, numerical framing, and manuscript preparation. The core scientific ideas, figures, and computations are the author’s own. The author takes full responsibility for all results.

## References

- [1] P. Kubelka and F. Munk, “Ein Beitrag zur Optik der Farbanstriche,” *Z. Tech. Phys.* **12**, 593–601 (1931).
- [2] P. Kubelka, “New contributions to the optics of intensely light-scattering materials. Part I,” *J. Opt. Soc. Am.* **38**, 448–457 (1948).
- [3] C. Zeller and R. Cordery, “Motzkin polynomial representations of Henyey–Greenstein scattering and Cauchy kernel asymptotics,” arXiv preprint (2025).
- [4] M. Hébert and R. D. Hersch, “Reflectance and transmittance model for recto-verso halftone prints,” *J. Opt. Soc. Am. A* **23**, 2415–2432 (2006).
- [5] M. Hébert, R. D. Hersch, and J.-M. Becker, “Compositional reflectance and transmittance model for multilayer specimens,” *J. Opt. Soc. Am. A* **24**, 2628–2644 (2007).
- [6] S. Mazaauric, M. Hébert, L. Simonot, and T. Fournel, “Two-flux transfer matrix model for predicting the reflectance and transmittance of duplex halftone prints,” *J. Opt. Soc. Am. A* **31**, 2775–2788 (2014).
- [7] M. Hébert, “Two-flux and multiflux matrix models for colored surfaces,” in *Handbook of Digital Imaging*, M. Kriss, ed. (Wiley, 2015).
- [8] L. Simonot, R. D. Hersch, M. Hébert, and S. Mazaauric, “Multilayer four-flux matrix model accounting for directional–diffuse light transfers,” *Appl. Opt.* **55**, 27–37 (2016).
- [9] J. L. Saunderson, “Calculation of the color of pigmented plastics,” *J. Opt. Soc. Am.* **32**, 727–736 (1942).
- [10] P. S. Mudgett and L. W. Richards, “Multiple scattering calculations for technology,” *Appl. Opt.* **10**, 1485–1502 (1971).
- [11] W. M. Star, J. P. A. Marijnissen, and M. J. C. van Gemert, “Light dosimetry in optical phantoms and in tissues: I. Multiple flux and transport theory,” *Phys. Med. Biol.* **33**, 437–454 (1988).
- [12] M. J. C. van Gemert and W. M. Star, “Relations between the Kubelka–Munk and the transport equation models for anisotropic scattering,” *Lasers Life Sci.* **1**, 287–298 (1987).
- [13] W. E. Vargas and G. A. Niklasson, “Applicability conditions of the Kubelka–Munk theory,” *Appl. Opt.* **36**, 5580–5586 (1997).
- [14] P. Edström, “Comparison of the DORT2002 radiative transfer solution method and the Kubelka–Munk model,” *Nord. Pulp Pap. Res. J.* **19**, 397–403 (2004).
- [15] S. Chandrasekhar, *Radiative Transfer* (Dover, New York, 1960).
- [16] J. H. Joseph, W. J. Wiscombe, and J. A. Weinman, “The delta-Eddington approximation for radiative flux transfer,” *J. Atmos. Sci.* **33**, 2452–2459 (1976).
- [17] W. J. Wiscombe, “The delta- $M$  method: rapid yet accurate radiative flux calculations for strongly asymmetric phase functions,” *J. Atmos. Sci.* **34**, 1408–1422 (1977).